

# Flow-Induced Patterning of Langmuir Monolayers

Michael J. Vogel,<sup>†</sup> Reza Miraghaie,<sup>‡</sup> Juan M. Lopez,<sup>§</sup> and Amir H. Hirsaa\*<sup>||</sup>

School of Chemical and Biomolecular Engineering, Cornell University, Ithaca, New York 14853, Mechanical and Aerospace Engineering Department, University of California, Los Angeles, California 90095, Department of Mathematics and Statistics, Arizona State University, Tempe, Arizona 85287, and Department of Mechanical, Aerospace and Nuclear Engineering, Rensselaer Polytechnic Institute, Troy, New York 12180

Received March 23, 2004. In Final Form: May 10, 2004

Insoluble monolayers on water have been patterned at the macroscopic scale (i.e., at the centimeter scale of the flow apparatus) as well as the mesoscopic scale (i.e., down to the micron scale resolvable via optical microscopy). The macroscopic patterning at the air/water interface results from a hydrodynamic instability leading to a steadily precessing flow pattern. The velocity field is measured, and the associated shear stress at the interface is shown to be locally amplified by the flow pattern. The resulting hydrodynamic effects on two different monolayer systems are explored: (1) the pattern in a model monolayer consisting of micron-size, surface-bound particles is visualized to show that the particles are concentrated into isolated regions of converging flow with high shear, and (2) Brewster angle microscopy of a Langmuir monolayer (vitamin K<sub>1</sub>) shows not only that the monolayer is patterned at the macroscopic scale but also that the localized high-shear flow further patterns the monolayer at the mesoscale.

There is wide interest in understanding the effects of hydrodynamics on monolayer structure both for fundamental reasons and for applications.<sup>1–7</sup> It is well-known that surfactant monolayers can significantly dampen fluid motion at the interface through the action of Marangoni stress as well as surface (excess) viscosity. Thus, unlike the case of clean liquid surfaces, where generating steady flow patterns such as Bénard–Marangoni convection cells<sup>8</sup> is relatively straightforward, spontaneous generation of patterns in monolayer-covered liquid surfaces is not common. In the case of Bénard flows, surfactant monolayers inhibit the occurrence of cells.<sup>9</sup> However, recent results show conditions under which surfactants can enable such patterns.<sup>10,11</sup> Our results in this Letter show that pattern formation via hydrodynamic instability can impart significant stress to the interface and that the resulting flow-induced patterns can be obtained in the presence of a surfactant monolayer. The interest in this is motivated by the potential to tailor the stress distribution in monolayers and in turn influence monolayer microstructure and macroscale response. By exploiting hydrodynamic symmetry-breaking bifurcations in laminar vortical flows, we are able to impart a wide range of shear distributions on the monolayer in a well-controlled fashion.

A flow in which the air/water interface is amenable to patterning is that in a stationary cylinder driven by the

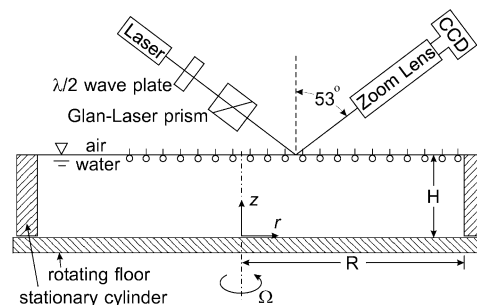


**Figure 1.** Schematic of the flow apparatus and Brewster angle microscope setup for imaging the Langmuir monolayer.

constant rotation of the floor at  $\Omega$  rad/s (Figure 1). Experiments were conducted with two cylinders of radius  $R = 2.5$  cm, one of height  $H = 0.66$  cm and the other 5.0 cm.<sup>12</sup> The bulk flow is completely characterized by two parameters: the height-to-radius ratio  $H/R$  and the Reynolds number  $Re = \Omega R^2/\nu$ , where  $\nu$  is the bulk fluid kinematic viscosity ( $\nu = 0.00946$  cm<sup>2</sup>/s for water<sup>13</sup> at 22.5 °C). The velocity in water and at the air/water interface was measured via digital particle image velocimetry (DPIV). The details, including procedures for cleaning the seeding particles<sup>14</sup> and the quality tests of the double-distilled water used in the experiments, were previously presented.<sup>15</sup>

For low  $Re$  ( $<10^3$ ) and large  $H/R$  ( $>1$ ), the flow is axisymmetric and steady with the bulk flow mostly in solid-body rotation and the shearing on the air/water interface localized in the cylinder boundary layer.<sup>16</sup> In such flows, monolayers on the interface remain essentially

\* To whom correspondence should be addressed. E-mail address: hirsaa@rpi.edu.

<sup>†</sup> Cornell University.

<sup>‡</sup> University of California, Los Angeles.

<sup>§</sup> Arizona State University.

<sup>||</sup> Rensselaer Polytechnic Institute.

(1) Schwartz, D. K.; Knobler, C. M.; Bruinsma, R. *Phys. Rev. Lett.* **1994**, *73*, 2841.

(2) Maruyama, T.; Fuller, G.; Frank, C.; Robertson, C. *Science* **1996**, *274*, 233.

(3) Dennin, M.; Knobler, C. M. *Phys. Rev. Lett.* **1997**, *78*, 2485.

(4) Kurnaz, M. L.; Schwartz, D. K. *Phys. Rev. E* **1997**, *56*, 3378.

(5) Igenes-Mullol, J.; Schwartz, D. K. *Langmuir* **2001**, *17*, 3017.

(6) Ding, J.; Warriner, H. E.; Zasadzinski, J. A. *Phys. Rev. Lett.* **2002**, *88*, 168102.

(7) Ghaskadvi, R. S.; Dennin, M. *Langmuir* **2000**, *16*, 10553.

(8) Pearson, J. R. A. *J. Fluid Mech.* **1958**, *4*, 489.

(9) Berg, J. C.; Acrivos, A. *Chem. Eng. Sci.* **1965**, *20*, 737.

(10) Nguyen, V. X.; Stebe, K. J. *Phys. Rev. Lett.* **2002**, *88*, 164501.

(11) Truskett, V. N.; Stebe, K. J. *Langmuir* **2003**, *19*, 8271.

(12) The top rims of the cylinders were made hydrophobic so that the contact line could be pinned and a flat interface could be obtained statically by completely filling the cylinder; precise details are given elsewhere.<sup>16</sup>

(13) Water was selected for the experiments because of the vast literature on insoluble monolayers on it, as well as its importance in biological applications.

(14) Polystyrene particles (Duke Scientific, 7520A) with a mean diameter of 21  $\mu$ m were used for the present experiments with DPIV.

(15) Hirsaa, A. H.; Lopez, J. M.; Miraghaie, R. *J. Fluid Mech.* **2001**, *443*, 271.

(16) Lopez, J. M.; Marques, F.; Hirsaa, A. H.; Miraghaie, R. *J. Fluid Mech.* **2004**, *502*, 99.

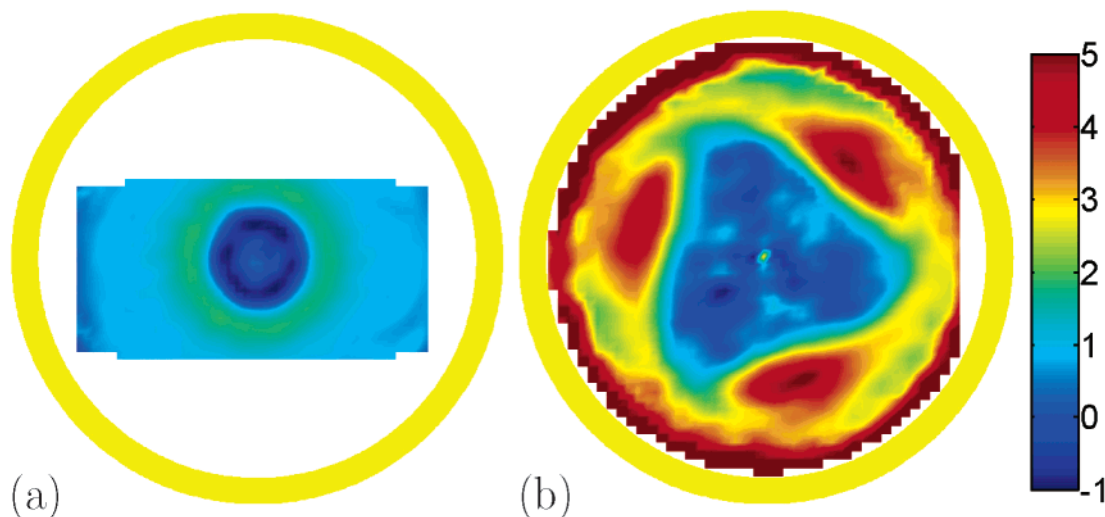


**Figure 2.** Shear stress  $\tau_{r\theta}$  ( $\text{s}^{-1}$ ) at the interface ( $z=H$ ) determined from velocity measurements made via DPIV: (a) an axisymmetric case with  $Re=1900$  and  $H/R=2.0$  and (b) a symmetry-broken case with  $Re=2000$  and  $H/R=0.26$ , both with vitamin  $K_1$  monolayers initially spread at  $c=0.8 \text{ mg/m}^2$ . The outline of the stationary cylinder is shown in yellow for reference. Note also that part a is cropped at the top and the bottom due to optical blockage<sup>16</sup> and that the jagged edge in part b is due to the rectilinear camera sensor and the subsequent DPIV analysis.

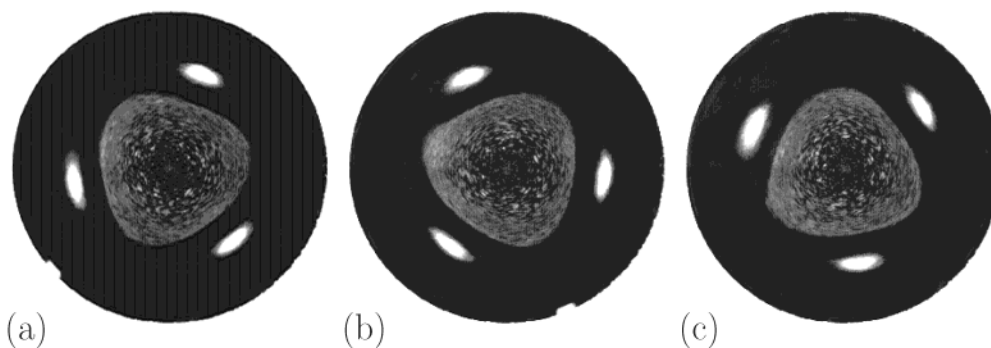


**Figure 3.** Photographs of surface-bound particles patterned (at the interface) by the three-dimensional hydrodynamic flow. Snapshots show the steadily precessing pattern at the air/water interface at phases  $T/3$  apart. These photos were taken  $\sim 1.5$  h after start-up. The small white tab visible at the cylinder wall (e.g. at 7 o'clock in part a) is attached to the bottom of the rotating floor for rotational reference.

uniformly distributed away from the cylinder wall. Either increasing  $Re$  or reducing  $H/R$  leads to symmetry breaking. From the perspective of patterning monolayers, a significant consequence of this symmetry breaking is that large shear and large gradients in shear are distributed throughout the interface in a very well-organized pattern that is steadily precessing; that is, the pattern is frozen in time. For example, with  $Re \sim 2000$  and  $H/R \sim 0.25$ , the nonaxisymmetric pattern has an azimuthal wavenumber  $m=3$  and precesses in the direction of the rotating floor with a period  $T=3.38/\Omega$ , which is about 1.1 s in this case. The steady precession means that looking at the pattern at a fixed azimuth  $\theta$  over a time  $T$  is equivalent to scanning along the azimuth from  $\theta=0$  to  $\theta=2\pi/3$  at a fixed time. Figure 2 shows the shear stress in the air/water interface,<sup>17</sup>  $\tau_{r\theta} = \rho\nu(\partial v_\theta/\partial r - v_\theta/r + 1/r \partial u_r/\partial \theta)$  (where  $\rho$  is the density of water) for (a) an axisymmetric case and (b) a nonaxisymmetric case, both with vitamin  $K_1$  (2-methyl-3-phytyl-1,4-naphthoquinone),<sup>20</sup> which forms an insoluble (Langmuir) monolayer on water, initially spread uniformly at a concentration of  $c=0.8 \text{ mg/m}^2$ . It should be noted that since the Froude number  $Fr = \Omega^2 R^2/gH$ , where  $g$  is the gravitational acceleration, is small, surface deformations are negligible and the interface remains flat for all practical purposes. Specifically, for the most critical case of small  $H$ , we have measured the maximum surface slope and found it to be insignificant ( $\sim 0.008$ ).<sup>16</sup>

The nonaxisymmetric shear stress distribution advects material on the air/water interface into distinct regions delineated by the stress pattern. To visualize its effects on the interface, we have repeated the experiment (at  $Re=2000$  and  $H/R=0.26$ ) with a model monolayer consisting of surface-bound and essentially surface-inactive particles;<sup>24</sup> images of these particles on the flowing interface are presented in Figure 3. Note that for  $r < 0.4$  the flow is in solid-body rotation with  $\tau_{r\theta} \approx 0$ , and the particles remain essentially uniformly distributed inside this

(17)  $\tau_{r\theta}$  is computed from DPIV data.<sup>18,19</sup>

(18) Miraghaie, R. Ph.D. Thesis, Department of Mechanical Engineering, Rensselaer Polytechnic Institute, 2002.

(19) Miraghaie, R.; Lopez, J. M.; Hirska, A. H. *Phys. Fluids* **2003**, *15*, L45.

(20) Vitamin  $K_1$  (Aldrich 28,740-7), which is liquid at room temperature, was diluted with hexane (Aldrich 13,938-6) and spread from a glass microsyringe. After the solution was spread, 15 min was allowed for the solvent to evaporate and for the monolayer to equilibrate. All the experiments were performed at  $22.5 \pm 0.5$  °C, where the monolayer is known to be well-behaved,<sup>21,22</sup> and its isotherms do not exhibit any measurable hysteresis—compressions and expansions are essentially identical and do not depend on initial and final concentration. We have also shown that vitamin  $K_1$  monolayers do not exhibit any measurable surface shear viscosity for  $c < 1.5 \text{ mg/m}^2$ .<sup>23</sup>

(21) Gaines, G. L. *Insoluble Monolayers at Liquid-Gas Interfaces*; Interscience: New York, 1966.

(22) Weitzel, G.; Fretzdorff, A.-M.; Heller, S. *Hoppe-Seyler's Z. Physiol. Chem.* **1956**, *303*, 14.

(23) Hirska, A. H.; Lopez, J. M.; Miraghaie, R. *J. Fluid Mech.* **2002**, *470*, 135.

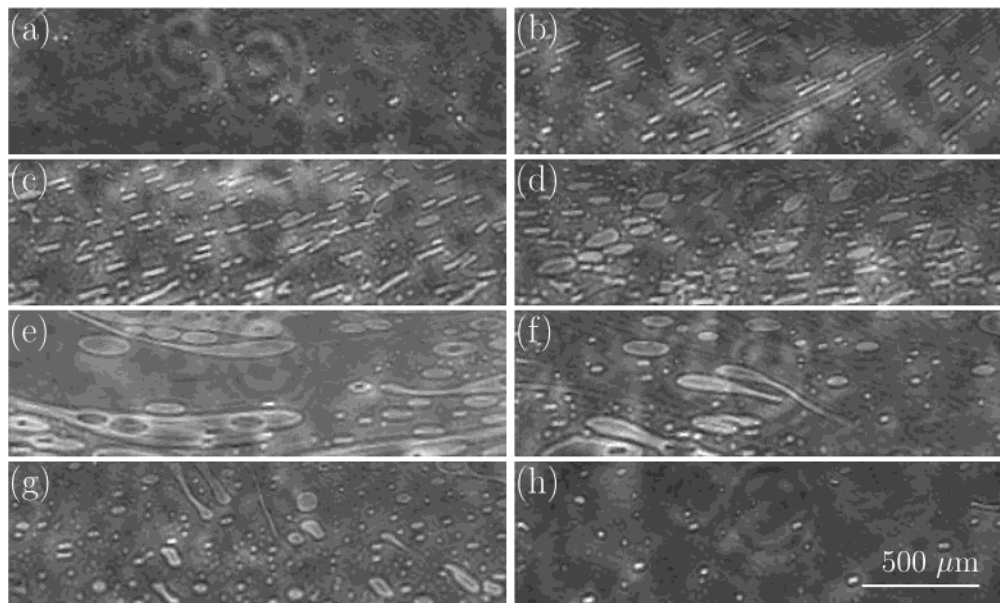


**Figure 4.** BAM images of the vitamin K<sub>1</sub> monolayer (initially uniformly spread to  $c = 0.4 \text{ mg/m}^2$ ) at  $r = 0.7R$  for  $Re = 2000$  and  $H/R = 0.26$ , taken at times (a)  $t_0$ , (b)  $t_0 + 0.06T$ , (c)  $t_0 + 0.22T$ , (d)  $t_0 + 0.32T$ , (e)  $t_0 + 0.41T$ , (f)  $t_0 + 0.57T$ , (g)  $t_0 + 0.73T$ , and (h)  $t_0 + 0.99T$ , where  $t_0$  is a reference time.

roughly triangular region of zero shear stress (cf. Figure 2b and Figure 3). For larger  $r$ , there are large gradients in  $\tau_{r\theta}$ , with large  $\tau_{r\theta}$  concentrated into three localized islands. Particles which were initially uniformly distributed at  $r > 0.5$  appear to have been advected into these high-shear regions. Surface tension measurements of the particles on water during compression in a Langmuir trough indicate that they do not form an elastic film, so there is no Marangoni stress opposing their accumulation.

The same experiment is now repeated using vitamin K<sub>1</sub> monolayers. To image the monolayer on the flowing system, we have devised a Brewster angle microscope (BAM) which utilizes a pulsed laser with a very short pulse duration to avoid smearing of a highly magnified monolayer image even though it may be flowing with a substantial velocity (of order 10 cm/s).<sup>25</sup>

The BAM images presented in Figure 4 were made at a fixed point of the interface, centered at  $r = 0.7R$ . This location was selected since it approximates the radial location of the three islands where particles had accumulated (see Figure 3). The camera orientation in the BAM setup (Figure 1) was such that the cylinder axis is toward the top of the page for the images shown in Figure 4. The sequence of images was taken during one period,  $T$ , which is the time it takes each satellite to reach the

initial position of the preceding satellite, that is, precess through an angle  $2\pi/3$ . The biphasic nature of the monolayer over this range of concentrations, consisting of coexisting liquid expanded (LE) phase domains (relatively dark) and liquid condensed (LC) domains (relatively bright), is apparent in the photographs. The periodicity of the BAM images presented in Figure 4 is consistent with the steadily precessing flow field, observed with the surface-bound particles on a clean surface (Figure 3), as well as the velocity field measurements made with the vitamin K<sub>1</sub> monolayer (Figure 2). Using the photograph in Figure 3b, for example, the structure of the monolayer shown in the time series of BAM images can be explained as follows. For illustration purposes, consider the arc region (at about  $r = 0.7R$ ) at about 5 o'clock, which corresponds to one apex of the shear-free triangle and is halfway between the islands at 7 o'clock and 3 o'clock in Figure 3b. Since the structures precess counterclockwise in the view used in all figures, the time series at a fixed location on the interface is equivalent to a clockwise-rotating arc along a snapshot of the surface. Thus, if the first BAM image (Figure 4a) is assumed to correspond to the 5 o'clock position in Figure 3b, then the last BAM image (Figure 4h) corresponds to about the 9 o'clock position. The region of maximum shear can be seen in parts d and e of Figure 4, which correspond to either side of the 7 o'clock position. These images also suggest that this region has the largest concentration due to the relatively larger percentage of the surface covered by the liquid condensed (bright) domains. Also note the asymmetry between the first four and the last four BAM images in Figure 4; the first four have domains which are much more fragmented (indicating much stronger shearing flow) than the last four. This is analogous to the  $\beta$  effect (cf. a tropical cyclone on the rotating Earth<sup>26</sup>), where the islands of high shear (due to the intense cyclonic flow) seen in Figure 2b reinforce the background azimuthal flow in the first four images and reduce it locally in the last four images. The resultant shear distribution is very nonuniform, and this is clearly evident in the way that the monolayer phase domains are fragmented and in the

(24) The surface-bound particles were obtained from 0.05 mL of 3  $\mu\text{m}$  polystyrene particles (Aldrich 45,941-0, 10% solid) in a 13 mL glass test tube by multiple rinses, centrifuging, and decanting with double-distilled water, followed by a methanol (Aldrich 27,047-4) rinse and subsequent rinses with double-distilled water. The resulting surface-bound particles were harvested from the top of the test tube, where they accumulated. Once the harvested particles are deposited on the surface of the clean water, they remain there despite any degree of agitation or flow.

(25) A frequency-doubled (532 nm) Nd:YAG laser (New Wave Research, Solo-1) producing 5 ns long pulses at a rate of 30 Hz was utilized. Thus, the movement of the monolayer during the laser pulse was less than a nanometer (compared to the 2 mm field of view) and was imperceptible. The schematic of the BAM is presented in Figure 1. The laser output was passed through a half waveplate (Thorlabs WPH05M-514) to obtain p polarized light, and a Glan polarizer removed any non-p polarized light ahead of the air/water interface. The reflected light was imaged using a lens system (Thales-Optem, 70XL, with a 2  $\times$  TV tube) mounted on a CCD camera (Texas Instruments, 1134P) with a 30 Hz frame rate. For all the images presented, the total magnification was 4 $\times$ .

(26) Anthes, R. A. *Mon. Weather Rev.* **1972**, *100*, 461.

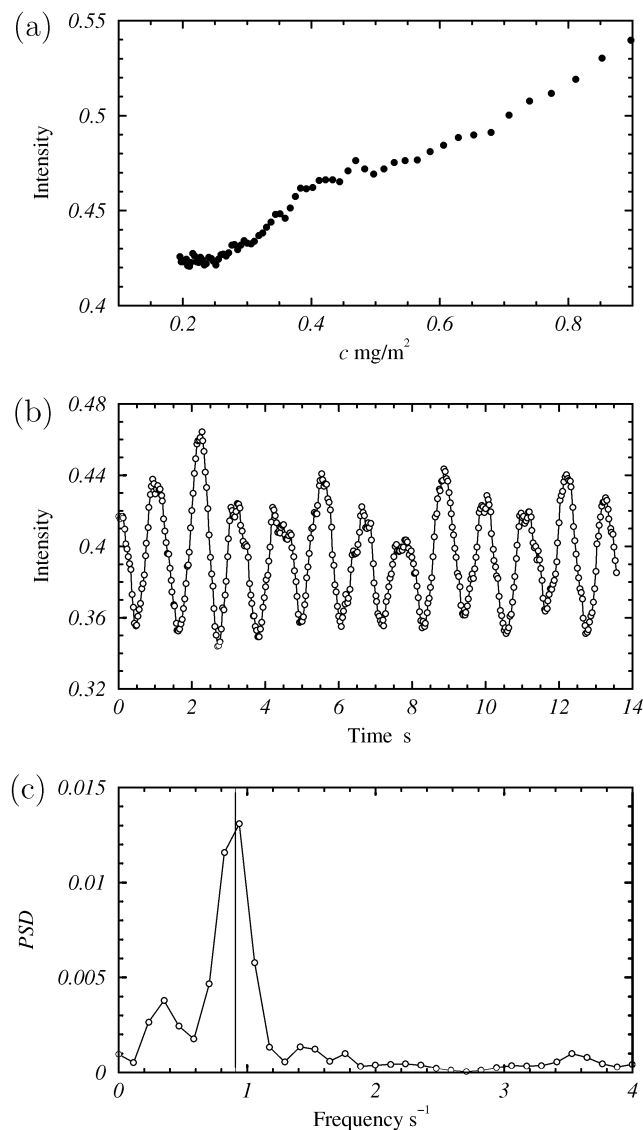


**Figure 5.** Measurements based on BAM images of vitamin  $\text{K}_1$  monolayers: (a) BAM intensity (on a scale of 0 to 1, where 0 is black and 1 is white) averaged over the image area as a function of monolayer concentration, obtained in a Langmuir trough during a slow compression; (b) time series of BAM intensity at  $r = 0.7R$  for a symmetry-broken case ( $Re = 2000$ ,  $H/R = 0.26$ ) with azimuthal periodicity  $m = 3$  and a vitamin  $\text{K}_1$  monolayer initially spread at  $c = 0.4 \text{ mg/m}^2$ ; (c) power spectral density of the time series in part b, using the last 256 data points, removing the mean, and using a Blackman window for the FFT. Note the precession frequency of the symmetry-broken case as determined from velocity measurements<sup>19</sup> is indicated in part c by the vertical line.

directions in which these fragments are aligned (locally aligned with the shear). Further, the large variation in relative areas of LE and LC domains is indicative of concentration variations in the azimuthal direction  $\theta$ , consistent with the converging flow near the three islands of high shear.

In general, precise knowledge of the monolayer concentration distribution is as yet unavailable in such flowing systems. However, the BAM images can be used to show qualitatively how the monolayer is macroscopically patterned by the flow. By averaging the light intensity over the BAM field of view, an indirect measure of the monolayer concentration was obtained for the vitamin  $\text{K}_1$  monolayer over the range of concentrations where coexisting phase domains are observed. This is illustrated in Figure 5a, where the BAM intensity (averaged over the field of view) is shown as a function of monolayer concentration during a slow compression in a Langmuir trough. The monolayer was compressed from an initial concentration of  $0.2 \text{ mg/m}^2$  to a final concentration of about  $1.6 \text{ mg/m}^2$  in about 10 min. Low concentrations give BAM images that are relatively dark (LE phase). As concentration increases, brighter small domains (LC phase domains) begin to appear and grow in number and size. At the highest concentrations, the BAM image is uniformly at the brighter intensity of the LC domains. The relationship between concentration and intensity is approximately linear in this range of concentration (Figure 5a). Thus, the average BAM intensity is indicative of the monolayer concentration in the flowing system. Figure 5b is a time series of the averaged BAM intensity, for a measurement centered at  $r = 0.7R$ , for a vitamin  $\text{K}_1$  monolayer initially spread at a concentration of  $0.4 \text{ mg/m}^2$  on the same flow as that in Figures 2b, 3, and 4 ( $Re = 2000$ ,  $H/R = 0.26$ ). Although there is substantial noise in the spatially averaged BAM signal, a periodic trend is apparent. The frequency can be found from the power spectral density (PSD) of the signal in Figure 5b. The PSD (Figure 5c) clearly shows a dominant peak at frequency  $\approx 0.94 \text{ Hz}$  as well as smaller peaks at the harmonics. This is in good agreement with the frequency of the pattern precession ( $1/T = 0.91 \text{ Hz}$ ) obtained from velocity measurements via DPIV and from flow visualization.<sup>19</sup> The small discrepancy (about 3%) is due to experimental uncertainties as well as the relatively small data set (256 points) used in the fast Fourier transform (FFT) calculation for the PSD.

On the basis of the measured velocity and corresponding strain fields (Figure 2b), it can be concluded that the monolayer must be macroscopically patterned due to the hydrodynamic coupling<sup>27,28</sup> between the interfacial and bulk flows. In other words, nonuniform surface stress requires a nonuniform monolayer concentration. Furthermore, our observations using BAM images present direct evidence of the flow-induced patterning of the Langmuir monolayer at the mesoscale.

**Acknowledgment.** We wish to thank Dr. Junqi Ding for assisting with the design and setup of our BAM system. This work was partially supported by the National Science Foundation.

LA0492355

(27) Slattery, J. C. *Interfacial Transport Phenomena*; Springer: New York, 1990.

(28) Edwards, D. A.; Brenner, H.; Wasan, D. T. *Interfacial Transport Processes and Rheology*; Butterworth-Heinemann: Boston, 1991.